Since January 2020 Elsevier has created a COVID-19 resource centre with free information in English and Mandarin on the novel coronavirus COVID-19. The COVID-19 resource centre is hosted on Elsevier Connect, the company's public news and information website.

Elsevier hereby grants permission to make all its COVID-19-related research that is available on the COVID-19 resource centre - including this research content - immediately available in PubMed Central and other publicly funded repositories, such as the WHO COVID database with rights for unrestricted research re-use and analyses in any form or by any means with acknowledgement of the original source. These permissions are granted for free by Elsevier for as long as the COVID-19 resource centre remains active.

European Journal of Medicinal Chemistry 161 (2019) 456–467

Contents lists available at ScienceDirect

European Journal of Medicinal Chemistry

journal homepage: http://www.elsevier.com/locate/ejmech

Research paper

ASR352, A potent anticancer agent: Synthesis, preliminary SAR, and biological activities against colorectal cancer bulk, 5-fluorouracil/oxaliplatin resistant and stem cells

Satya Narayan [a, **], Srinivasa Ramisetti [b], Aruna S. Jaiswal [c], Brian K. Law [d], Ashona Singh-Pillay [e], Parvesh Singh [e], Shantu Amin [b], Arun K. Sharma [b, *]

[a] Department of Anatomy and Cell Biology, University of Florida, Gainesville, FL, 32610, USA
[b] Department of Pharmacology, Penn State University College of Medicine, Penn State Cancer Institute, Hershey, PA, 17033, USA
[c] Department of Hematology and Oncology, University of Florida, Gainesville, FL, 32610, USA
[d] Department of Pharmacology and Experimental Therapeutics, University of Florida, Gainesville, FL, 32610, USA
[e] School of Chemistry and Physics, University of Kwa-Zulu Natal (UKZN), Westville Campus, Durban, 4000, South Africa

ARTICLE INFO

Article history:
Received 3 July 2018
Received in revised form
7 October 2018
Accepted 22 October 2018
Available online 23 October 2018

Keywords:
Colorectal cancer
Stem cells
Tetraazaadamantane
Apoptosis
Checkpoint kinase 1

ABSTRACT

Despite new agent development and short-term benefits in patients with colorectal cancer (CRC), metastatic CRC cure rates have not improved due to high rates of 5-fluorouracil (5-FU)/leucovorin/oxaliplatin (FOLFOX)-resistance and a clinical therapeutic plateau. At the same time, this treatment regime leads to significant toxicity, cost, and patient inconvenience. Drug-resistance is linked to CRC stem cells, which are associated with the epidermal-to-mesenchymal transition (EMT) pathway. Thus, to optimally treat CRC, a therapy that can target the cell survival and EMT pathways in both CRC bulk and stem cell populations is critical. We recently identified a novel small molecule NSC30049 (**7a**) that is effective alone, and in combination potentiates 5-FU-mediated growth inhibition of CRC bulk, FOLFOX-resistant, and CRC stem cells both *in vitro* and *in vivo* models. In the present study, we report the synthesis and anti-CRC evaluation of several stable and effective **7a** analogs. ASR352 (**7b**) was identified as one of the equipotent **7a** analogs that inhibited the growth of CRC bulk cells, sensitized FOLFOX-resistant cells, and reduced the sphere formation capacity of CRC stem cells. It appears that the complex mechanism of cytotoxicity for **7b** includes abrogation of 5-FU-induced the S phase, reduction of the phosphorylation of Chk1 at S317P, S345P and S296P, increased γH2AX staining, activation of caspase 3/PARP1 cleavage, and enhancement of Bax/Bcl2 ratio. Further **7b**-mediated reduced phosphorylation of Chk1 was an indirect effect, since it did not inhibit Chk1 activity in an *in vitro* kinase assay. Our findings suggest that **7b** as a single agent, or in combination with 5-FU can be developed as a therapeutic agent in CRC bulk, FOLFOX-resistant, and CRC stem cell populations for unmanageable metastatic CRC conditions.

© 2018 Elsevier Masson SAS. All rights reserved.

1. Introduction

Despite the attempts to improve patient outcomes by incorporating new active systemic agents into clinical practice, there has been little improvement in the metastatic CRC patient cure rate. In spite of 5-fluorouracil (5-FU) use, with or without additional therapy, to eradicate metastatic disease after "curative" surgery for CRC, most cancers relapse within the first few years following treatment completion. This suggests that there is a relatively rapid repopulation of neoplastic progeny, i.e., CRC stem cells [1,2]. A more aggressive treatment with higher or prolonged doses of multiple drug combinations, such as 5-FU and oxaliplatin, leads to serious side-effects [3,4]. Despite the frequent use of 5-FU in cancer, a thorough understanding of its mechanisms of action and interventions to overcome resistance are still relatively limited. One of mechanisms of resistance to 5-FU occurs through the induction of the EMT pathway [5,6]. The down-regulation of epithelial markers (APC, β-catenin and E-cadherin) is characteristic to the EMT pathway EMT, which is involved in CRC stem cell invasion,

* Corresponding author.
** Corresponding author.
E-mail addresses: snarayan@ufl.edu (S. Narayan), asharma1@pennstatehealth.psu.edu (A.K. Sharma).

https://doi.org/10.1016/j.ejmech.2018.10.052
0223-5234/© 2018 Elsevier Masson SAS. All rights reserved.

metastasis and drug-resistance [7–12].

In an effort to develop a more effective drug that has a minimal side effect profile on normal epithelial cells in CRC treatment, we recently identified a novel tetraazaadamantane containing small molecule NSC30049 (1-(4-Chloro-2-butenyl)-1λ~5~,3,5,7-tetraazatricyclo[3.3.1.1–3,7~]decane) that either alone or in combination potentiates 5-FU-mediated growth inhibition of CRC heterogeneous bulk, FOLFOX-resistant and CRC stem cells while maintaining the integrity of the normal colonic epithelial cells [13]. Nitrogen containing adamantane analogs [14,15], e.g., 1-azaadamantanes, 1,3-diazaadamantanes, 1,3,5-triazaadamantanes and 1,3,5,7-tetraazaadamantanes are of great interest as conformationally constrained motifs for the design of various pharmacological tools [16]. Structural uniqueness of these azaadamantanes is related to both physical and chemical properties, most notably in the reduction of lipophilicity thus inducing higher aqueous solubility of these compounds compared to that of adamantanes consisting solely of carbon and hydrogen atoms [14,15]. However, studies of the biological activity of azaadamantanes and their derivatives are still relatively less explored despite having good pharmacological properties. A few representative examples of 1-azaadamantane motif (Fig. 1) include 5-HT4 receptor agonist SC-54750 (**1**) [17], a modulator of neuronal nicotinic acetylcholine receptors (nAChRs) **2** [18–20], inhibitors of σ_1 (CNS related diseases) and σ_2 (cancer), inhibitors of human T-cell leukemia virus-1 (HTLV-1), and anti-viral and analgesic agents [21–23]. Furthermore, the natural product, ansabananin (ABN) (**3**) that inhibits SARS Coronavirus (SCV) [24], and other natural alkaloids dapholdamine B (**4**) [25], daphnezomines A (**5**) [26] possess 1-azaadamantane moiety (Fig. 1). Recently, a diazaadamantane derivative **6** has been reported as an inhibitor of the rimantadine-resistant strain of the influenza A/Puerto Rico/8/34 (H1N1) virus [27]. It is noteworthy that although methenamine is clinically used to prevent urinary tract infections [28], the tetrazaadementane skeleton is barely utilized to design small drug-like molecules except in synthesizing the crucial reaction intermediate phenacyl amines [29–31]. NSC30049 (**7a**) is a unique tetraazaadamentane (methenamine) analog identified recently by our group that showed activity against 5-FU/oxaliplatin resistant and stem cells [13].

The expected mechanism of action of **7a** in CRC is through the inhibition of checkpoint kinase 1 (Chk1) pathway through an indirect mechanism(s) [13]. Since Chk1 plays a critical role in cell cycle regulation in response to DNA damage, several Chk1 inhibitors have been developed and tested as chemo-sensitizing agents [32–39]. Compound **7a** has been shown to inhibit Chk1 phosphorylation both *in vitro* and *in vivo* CRC models [13]; however, the pharmacokinetic analysis showed a short plasma half-life similar to 5-FU [40]. The short plasma half-life of **7a** is likely due to the presence of a reactive alkyl chloride group. To overcome this problem, we designed and synthesized several novel tetraazaadamantane **7a** analogs, and tested their cytotoxic efficacy against CRC bulk, FOLFOX-resistant as well as CRC stem cells.

2. Results and discussion

2.1. Design

The structural optimization of **7a** was focused mainly on replacing the reactive alkyl chloride group with more stable alkyl/alkenyl/aryl moieties. The rationale is that reactive alkyl chloride can potentially react with protein thiols and amines to compromise its plasma half-life and thus the biological activity. The functionalities that replaced cholo (Cl) group were chosen to enhance the overall stability of the molecule while retaining or possibly enhancing the potency (Fig. 2). In addition, the approaches of modification also included saturation of the olefinic group, shortening of the alkyl chain length, and replacement of nitrogen (N-7) of tetraazaadmantane ring with phosphorus having more labile valence shell electrons (Fig. 2).

2.2. Chemistry

Novel 1,3,5,7-tetraazaadamantane (**7a-c, g, f** & **11a-c)** and 1,3,5-triaza-7-phosphaadamantane (**7d-f)** analogs of NSC30049 (**7a**) were prepared as depicted in Schemes 1 and 2. Compounds **7a-c**

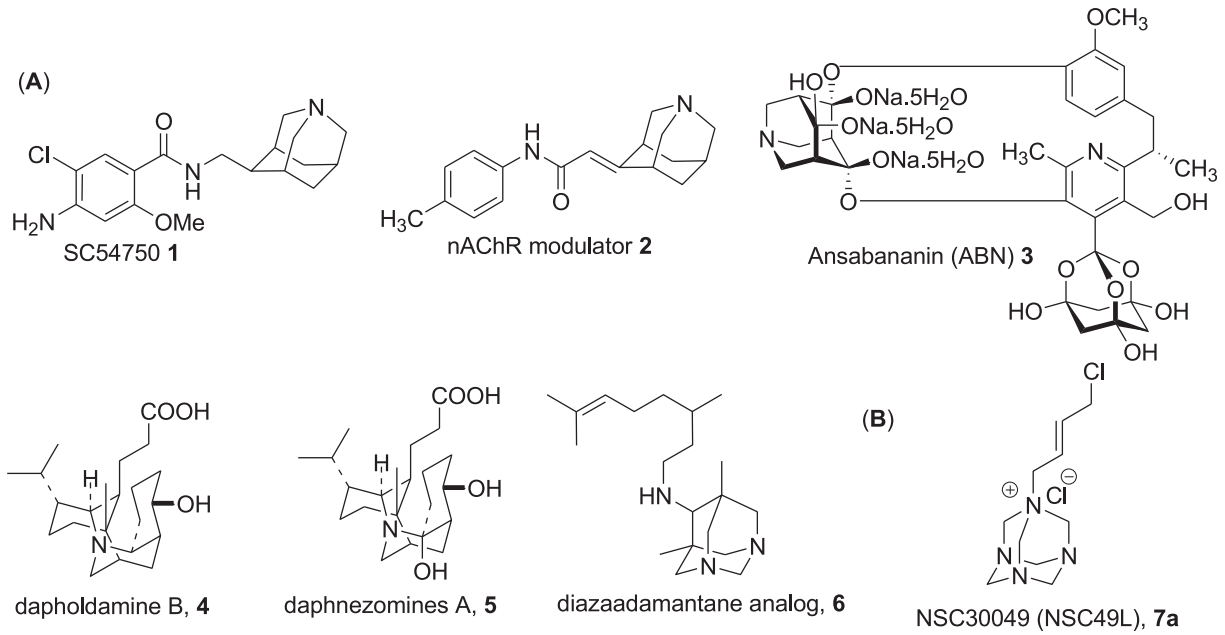

Fig. 1. Panel A shows the structure of pharmacologically important natural and synthetic azaadamantane compounds. **Panel B** is the structure of the lead tetraazaadamantane Chk1 inhibitor **7a**.

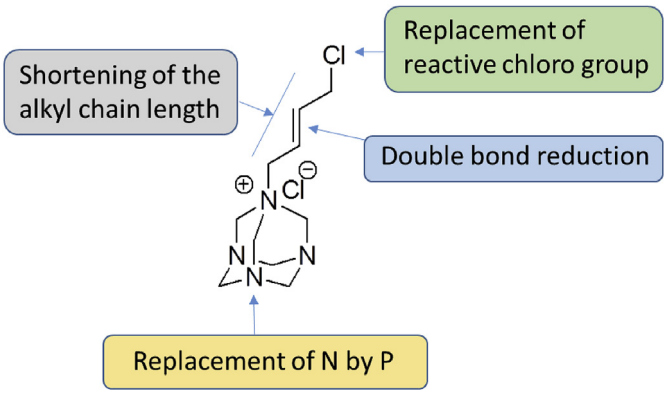

Fig. 2. Optimization strategy for **7a.**

were synthesized by the reaction of readily available tetraazaadamantane **8a** with various alkenyl halides **9a-c** in CH_2Cl_2 under reflux conditions in quantitative yields (Scheme 1) [41]. To evaluate the difference in activity between the nitrogen and corresponding phosphorus analogs, we also synthesized isosteric 7-phosphorus analogs (**7d-f**) of lead compound **7a**. 1,3,5-Triaza-7-phophaadamanatne **8b** was reacted under reflux conditions in CH_2Cl_2 with different alkenyl halides **9a-c** to furnish the corresponding phosphorus analogs **7d-f** in excellent yields (Scheme 1). Butyl chloride analog **7g** and the boronic acid analog **7h** were also synthesized using similar reaction conditions by refluxing for 12 h and 24 h, respectively.

To further diversify the structure activity relationship study on azaadamantane **7a** derivatives, we synthesized azaadamantane analogs **11a-c** as depicted in Scheme 2. Compounds **11a-c** were synthesized by reacting **8a** with readily available phenacyl chlorides **10a-c** in CH_2Cl_2 under reflux conditions in good yields (Scheme 2) [41]. The structures of all the novel NSC30049 derivatives were confirmed by ^1H NMR, ^{13}C NMR and HRMS analysis. The compounds purity (≥98%) was analyzed by analytical high-performance liquid chromatography (HPLC) before proceeding for *in vitro* biological assays.

2.3. Biology

2.3.1. Cytotoxicity evaluation of novel azaadamantane: ASR352 (7b) induces cytotoxicity and reduces the effective concentration of 5-FU in CRC cells

We determined the IC_{50} of the novel azaadamantane (**7a-c, g, h** and **11a-c**) and aza-phosphaadamantane (**7d-f**) analogs of NSC30049 (**7a**) in HCT116 cells by MTT-cell survival assay. Results showed a variable range of IC_{50} of these analogs. Based on the results of this cell viability assay, some structure-activity relationship (SAR) can be inferred: First, reducing the olefinic double bond by retaining chlorine atom (**7g**) reduced the potency of the

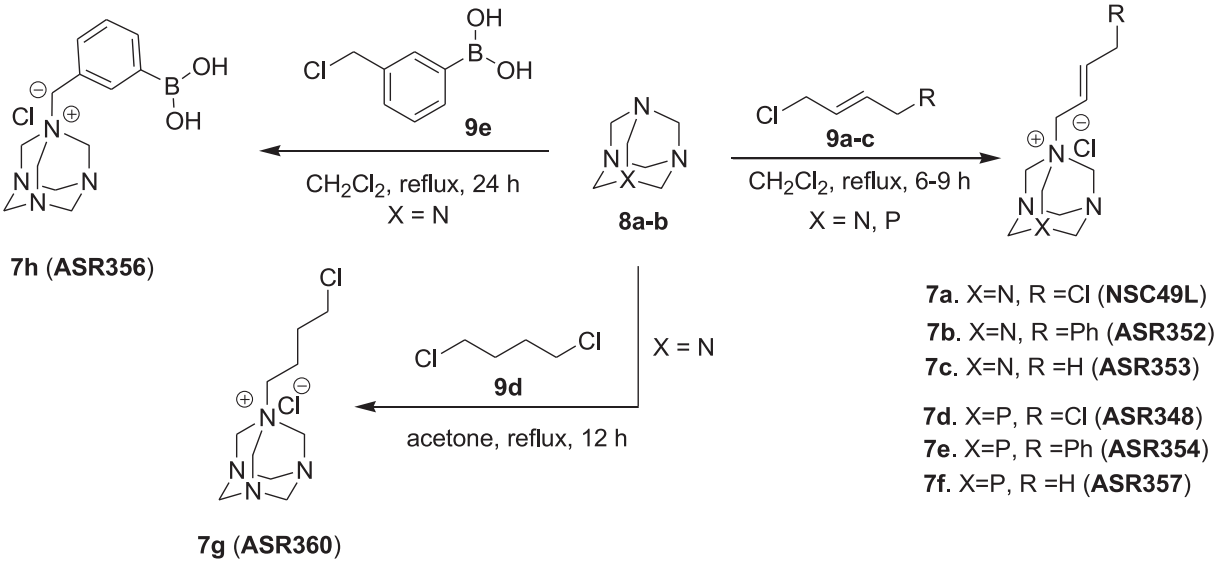

Scheme 1. Synthesis of 1,3,5,7-tetraaza- and 1,3,5-triaza-7-phospha-adamentane derivatives (**7a-h**).

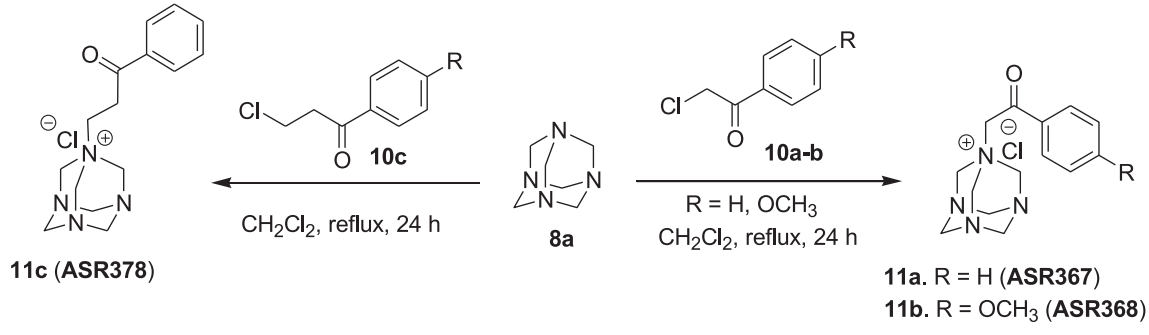

Scheme 2. Synthesis of 1,3,5,7-tetrazaadamentane phenacyl derivatives (**11a-c**).

compounds on cancer cell viability. Second, replacing the chlorine atom of **7a** by a phenyl (ASR352, **7b**) retained the activity of the molecule while the removal of the chlorine atom (**7c**) led to reduced potency (Table 1). Third, isosteric phosphorous analogs of **7a** (i.e. **7d**) and **7b (**i.e. **7e)** displayed only moderate cell viability when compared to its parent nitrogen analogs, while both **7c** and its isosteric phosphorus analog **7h** exhibited poor activity (Table 1). Compound **7h** having a 3-phenyl boronic acid functionality also led to a reduced potency. Fourth, among the analogs designed by replacing chlorine atom of **7a** with phenacyl groups of different alkyl chain lengths (**11a-c**), analogs having phenyl (ASR367, **11a**, IC_{50} 18.53 ± 1.41 μM) and 4-methoxy phenyl (**11b**, IC_{50} 13.10 ± 0.16 μM) displayed moderate inhibition of cell viability, while **11c** designed by extending the alkyl chain length of **11a** lost the activity (Table 1). Overall, except replacement of Cl^- group of **7a** by a phenyl group, all other modifications in structure including chain length, functional group variation, or isosterically replacing nitrogen by phosphorous, caused a dramatic reduction in or the total loss of cytotoxicity against HCT116 cells (Table 1). Compounds **7d**, **11a** and **11b** showed IC_{50} in the range of 13–18 μM; other analogs, such as **7c**, **7e**, **7f**, **7h**, **7g** and **11c** did not show any or very poor inhibitory activity against HCT116 cells (Table 1).

Among all these analogs, **7b** exhibited a low micromole range IC_{50} (5.75 ± 0.09 μM) that was close to the IC_{50} of **7a** (2.46 ± 0.14 μM) (Table 1). Thus, **7b** was identified as the lead novel compound having potency comparable to **7a**. This result suggests that the Cl^- of the **7a** is not an active group responsible for the cytotoxic activity of this compound and **7b** appears pharmacologically more stable and favorable for further development.

Next, we determined whether **7b** can enhance the potency of 5-FU in CRC cells. Results showed that the **7b** treatment reduced the IC_{50} of 5-FU with HCT116 and HT29 cell lines in a dose-dependent manner that was similar to **7a** (Table 2). These results indicate that **7a** and its analog **7b** can reduce the effective dose of 5-FU and inhibit the growth of all CRC cells, thus potentiating the effect of current therapy.

2.3.2. Compound 7b inhibits the growth of FOLFOX-HCT116 and FOLFOX-HT29 cells with similar efficiency as 7a

To determine whether **7b** can inhibit the survival of FOLFOX-resistant HCT116 and HT29 cell lines [42], we performed MTT-cell survival assay and compared the results with **7a**. Indeed, treatment with **7b** effectively sensitized both FOLFOX-HCT116 and FOLFOX-HT29 cell lines with an IC_{50} of 2.38 ± 0.25 μM and 2.59 ± 0.28 μM, respectively, that was similar to or slightly better than the IC_{50} of **7a**; IC_{50} of **7a** was 5.50 ± 0.20 μM and 3.08 ± 0.09 μM, respectively, for FOLFOX-HCT116 and FOLFOX-HT29 cell lines (Table 3). Since the growth of FOLFOX-resistant HCT116 and HT29 cell lines are maintained in the continuous presence of 50 μM 5-FU and 1.25 μM oxaliplatin, the effect on reduced IC_{50} of **7b** and **7a** with these cell lines is independent of 5-FU and oxaliplatin treatments.

Table 1
Screening of NSC30049 (**7a**) analogs for their toxicity with HCT116 cells.

Compounds	IC_{50} (μM)[a]
7a	2.46 ± 0.14
7b	5.75 ± 0.09
7c	ND
7d	18.39 ± 2.79
7e	ND
7f	ND
7h	ND
7g	ND
11a	18.53 ± 1.41
11b	13.10 ± 0.16
11c	ND

[a] The IC_{50} of different analogs was determined by MTT-cell survival assay. Data is the mean ± SE of four estimations. ND, not detectable.

2.3.3. Compound 7b inhibits the spheroid formation capacity of CA2 cells

In recent studies we have shown that **7a** inhibits the spheroid formation activity of CRC stem cells [13]. Here, we determined whether **7b** has similar activity against CRC stem cells. For these experiments, we used a well-characterized CRC stem cell line, CA2 [43,44] and performed sphere formation assays involving three-dimensional (3D) culture system in serum-free conditions. Results showed that **7b** inhibited the growth of spheres similar to **7a** (Table 3). The IC_{50} of **7b** in CA2 cells were greater than the IC_{50} of heterogeneous population of CRC bulk cell lines HCT116 and HT29, suggesting that CA2 cells are more resistant to these drugs than CRC bulk cells.

2.3.4. Compound 7b abrogates S phase arrest of HCT116 cells

In recent years many anticancer drugs have been discovered that target cell cycle checkpoints, arrest cell proliferation, and at the same time, provides opportunity for the repair of the damaged DNA [45,46]. The consequence of this leads to drug resistance and cell survival [47,48]. Therefore, current efforts are to induce death of the arrested cells by using inhibitors of the checkpoint kinases [49–51]. It was known that the therapeutic activity of 5-FU is linked to the replication stress as one of the mechanisms [52,53]. Several other inducers of the replication stress pathways have been implicated as therapeutic agents [51,53–56]. By enhancing replicative stress through perturbing the S-G_2/M checkpoints in cancer cells, a mitotic catastrophe can be induced with accumulated single-stranded DNA (ssDNA), and double-stranded DNA (dsDNA) breaks, that exceeds the repair capacity of the cell; and leads to cell death [57–59].

In recent studies, we have shown that **7a** treatment further increases S phase arrest of the cell cycle over hydroxyurea (HU) treatment [13], which is a pure inducer of replication stress-dependent S phase arrest [60,61]. In the present study, HCT116 cells were treated with 25 μM of 5-FU for 24 h, then with 20 μM of **7a** or **7b** for additional 8 h (Fig. 3A). The cell cycle analysis results showed 5-FU-induced S phase arrest of HCT116 cells (Fig. 3B). However, after combination treatment with **7a**, while S phase arrest continued the G_2/M phase arrest was abrogated. Interestingly, in combination with 5-FU, **7b** abrogated the S phase and increased the G_2/M phase arrest (Fig. 4B). The structural differences in **7a** and **7b** seem to be important for the differential activity of these two compounds on cell cycle profiling.

2.3.5. Compound 7b blocks HU-induced phosphorylation of Chk1 in HCT116 cells

Chk1 after phosphorylation at S317 subsequently phosphorylates itself at S345 for efficient progression of DNA replication forks and prevention of fork stalling. Therefore, to impair DNA repair or cellular division, Chk1 (S317P) inhibitors as single agent or in combination with chemotherapeutic agents may be important for further research. It is well-established that ATR-mediated Chk1 phosphorylation at S317P and S345P plays a critical role in DNA replication, DNA repair, S-G_2/M phase checkpoint control [62], and has been the target for cancer therapy [63], It has been also shown that the inhibition of Chk1(S317P) and Chk1(S296P) abrogates S-phase progression [64,65]. Since **7b** abrogates S phase arrest, we determined the phosphorylation level of Chk1 after treatment with **7b** either alone or in combination with HU, a pure inducer of S

Table 2
IC_{50} of 5-FU in the presence of **7a** and **7b** with HCT116 and HT29 cell lines.

IC_{50} (μM)[a]		
Treatments	HCT116 cells	HT29 cells
5-FU	15.16 ± 4.20	16.45 ± 2.627
5FU + 0.5 μM **7a**	7.05 ± 0.79	8.12 ± 0.14*
5FU + 1 μM **7a**	6.27 ± 0.6*	7.38 ± 0.29*
5FU + 0.5 μM **7b**	8.19 ± 0.05*	8.52 ± 0.49*
5FU + 1 μM **7b**	7.56 ± 0.05*	6.57 ± 0.36*

[a] The IC_{50} of **7a** and **7b** was determined by MTT-cell survival assay. Data is the mean ± SE of four estimations. * = Significantly different than 5-FU alone.

Table 3
IC_{50} of **7a** and **7b** with FOLFOX-HCT116, FOLFOX-HT29 and CA2 cell lines.

IC_{50} (μM)[a]			
Compounds	FOLFOX-HCT116 cells	FOLFOX-HT29 cells	CA2 cells
7a	5.50 ± 0.20	3.08 ± 0.09	7.96 ± 1.03
7b	2.38 ± 0.25	2.59 ± 0.28	9.06 ± 0.71

[a] The IC_{50} of **7a** and **7b** was determined by MTT-cell survival assay with FOLFOX-HCT116 and FOLFOX-HT-29 cell lines and by spheroid formation assay with CA2 cells. Data is the mean ± SE of three estimations.

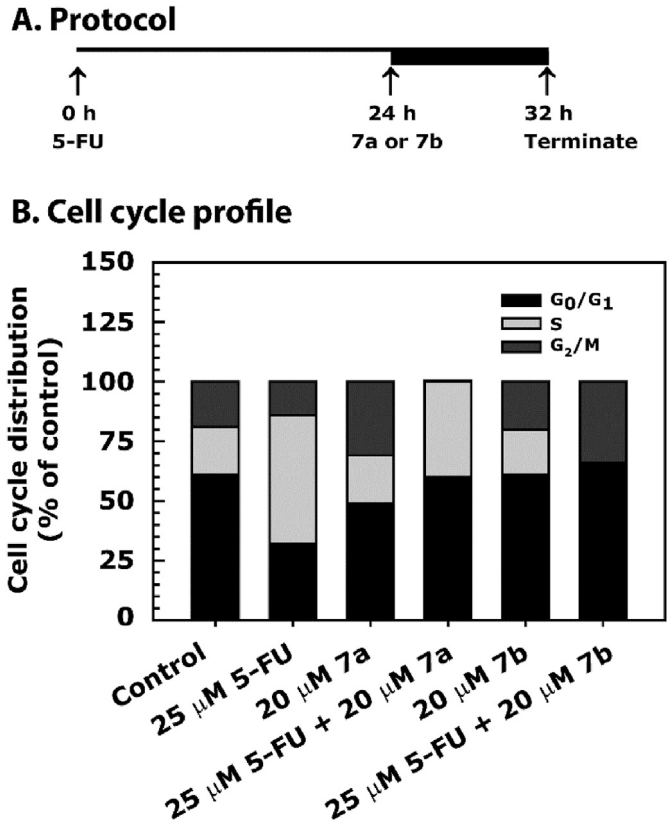

Fig. 3. Cell cycle profile of HCT116 cell line-treated with 7a and 7b either alone or in combination with 5-FU. Panel A describes the assay protocol. **Panel B** shows the data as a stacked bar graph. Cells were grown in 0.5% FBS for 20 h and then treated with 25 μM of 5-FU for 24 h, followed by treatment with 20 μM of **7a** or **7b** for an additional 8 h. After treatment, cells were processed for cell cycle analysis by FACS analysis. The ranges for G_0/G_1, S and G_2/M-phase arrested cells were established on the basis of the corresponding DNA content of the histograms. Data are mean percent distribution of DNA content of two different experiments.

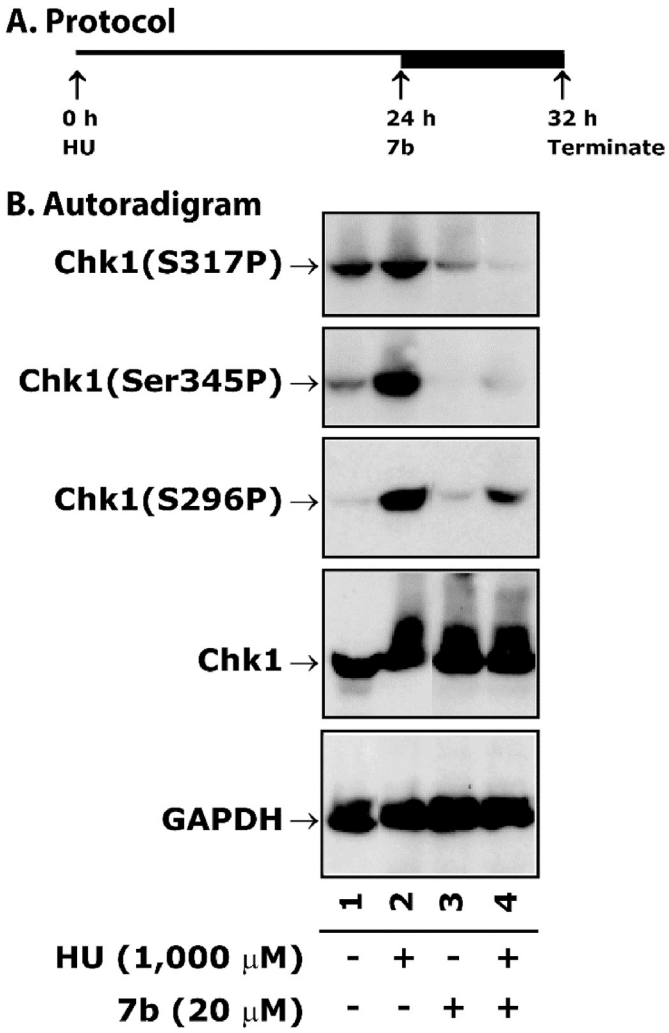

Fig. 4. Treatment of 7b inhibits HU-induced phosphorylation of Chk1 in HCT116 cells. Panel A depicts the protocol of the assay. Cells were treated with 1 mM of HU for 24 h followed by 20 μM of **7b** for an additional 8 h. **Panel B** shows representative autoradiograms of Chk1 western blots analyzed with whole cell extract. Normalization of protein loading was assessed by GAPDH.

phase arrest [60,61]. The experimental protocol is described in Fig. 4A. Results showed a high level phosphorylation of Chk1(S317P), Chk1(S345P) and Chk1(S296P) after the treatment with HU (Fig. 5 compare lane 1 with 2)' which was reduced after

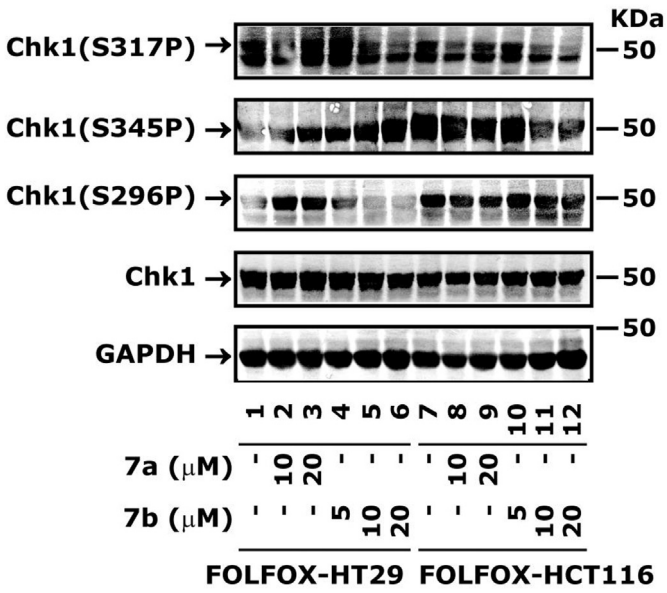

Fig. 5. Treatment of 7a and 7b inhibit Chk1 in FOLFOX-HT29 and FOLFOX-HCT116 cells. Cells were treated with different concentrations of **7a** and **7b** for 24 h. The whole cell extract was processed for the determination of Chk1 levels by western blot analysis. Normalization of protein loading was assessed by GAPDH.

combination treatment with **7b** (Fig. 4, compare lane 2 with 4). However, treatment with **7b** alone did not affect the phosphorylation of Chk1 (Fig. 4, compare lane 1 with 3). These results suggest that **7b** blocks HU-induced Chk1 phosphorylation and thus is involved in the abrogation of S phase as seen in Fig. 4.

2.3.6. Compound 7b blocks Chk1 phosphorylation in FOLFOX-HCT116 and FOLFOX-HT29 cell lines

We determined whether **7a** and **7b** can also block Chk1 phosphorylation, as observed with bulk HCT116 cells. The FOLFOX-HCT116 and FOLFOX-HT29 cell lines were treated with different concentrations of **7a** and **7b** for 24 h. The results showed inhibition of Chk1(S317P) and Chk1(S296P) in a dose-dependent manner (Fig. 5), as seen with bulk cells (Fig. 4B). There was an increase in Chk1(S345P) phosphorylation by both **7a** and **7b** with FOLFOX-HT29 cells; however, with FOLFOX-HCT116 cells it was reduced in a dose-dependent manner (Fig. 5). This differential effect of **7a** and **7b** on these two cell lines may be due to their p53 status, where FOLFOX-HT29 cells express mutant p53 and FOLFOX-HCT116 cells express wild-type p53. However, the mechanism by which p53 might be regulating Chk1 phosphorylation in these two cells lines is currently unknown.

2.3.7. Compound 7b induces double-stranded break of DNA in HCT116 cells, both as a single agent and in combination with 5-FU

Blockage of replication from UV, hydroxyurea, or 5-FU treatment activates the ATR-Chk1 pathway, stalls replication fork, and leads to double-stranded DNA breaks (DSBs), cell cycle arrest and apoptosis [66,67]. ATR phosphorylates histone H2A variant H2AX at Ser139 to form γH2AX that is considered as a marker of DSBs [68,69]. Previously, it has been shown that the inhibition of Chk1 by gemcitabine and 5-FU treatments increases γH2AX levels through ATR-mediated replicative stress [66,68]. In the present study, we examined whether **7b**-induced toxicity either alone or in combination with 5-FU, was related to DSBs and phosphorylation of γH2AX. We examined the levels of γH2AX by IHC staining. The cells treatment protocol is given in Fig. 6A. We observed an increased γH2AX-foci after treatment with **7b** alone in HCT-116 cells that was further increased in combination with 5-FU (Fig. 7B). Thus, these results show that **7b** either alone or in combination with 5-FU induces replication stress-mediated DNA damage in HCT-116 cells.

2.3.8. Compounds 7a and 7b do not inhibit Chk1 activity in a reconstituted purified system.

While from our cell-based studies it was clear that **7a** and **7b** inhibit Chk1 phosphorylation in FOLFOX-HCT116 and FOLFOX-HT29 cells, we do not know whether the inhibition of Chk1 phosphorylation by **7a** and **7b** was through direct or indirect mechanisms. For direct mechanism, we performed *in vitro* Chk1 kinase assay by using purified Chk1 protein. Results showed no inhibition of the Chk1 activity by any of these compounds (Table 4). Next, we tested whether any other kinases may be a target of these compounds. We profiled the activity of 366 kinases in an *in vitro* assay system but did not find a significant inhibition by **7a** and **7b** (see Table S1, *Supplementary Material*). From these results it became clear that the inhibition of Chk1 phosphorylation is not directly caused by **7a** and **7b**, but possibly due to some unknown mechanism(s) which remain to be elucidated.

ATR is one of the key activators of Chk1 phosphorylation at Ser345 and Ser317 [70], which promotes autophosphorylation of the same kinase at Ser296 that plays an important role in cell cycle control and DNA replication [71]. In our studies, the inhibition of

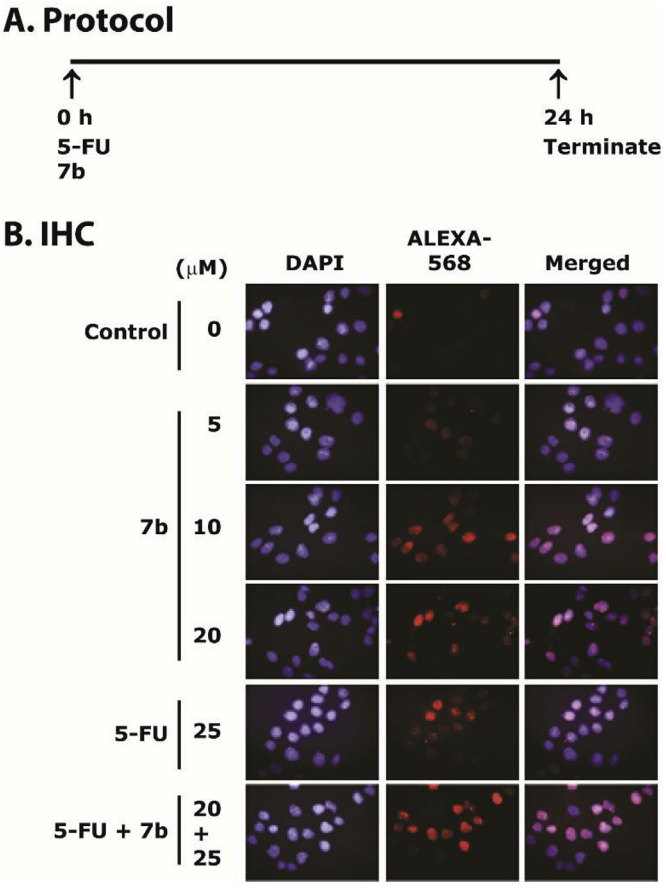

Fig. 6. Compound 7b and 5-FU treatments increase γH2AX-foci in HCT116 cells. Panel A describes the protocol of the assay. **Panel B** shows the IHC staining of γH2AX-foci formation (red) in nuclei of HCT-116 cells treated with **7b** (0, 5, 10 and 20 μM), 5-FU (25 μM) and combination of 5-FU (25 μM) and **7b** (20 μM) for 24 h. Magnification = 40×. (For interpretation of the references to color in this figure legend, the reader is referred to the Web version of this article.)

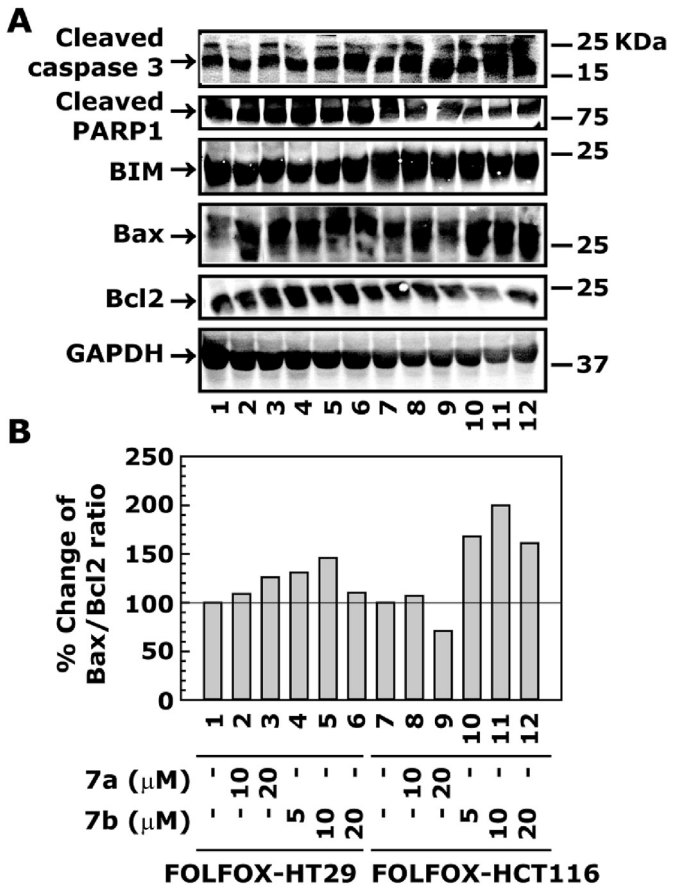

Fig. 7. Effect of 7a and 7b treatments on the expression of apoptotic marker proteins in FOLFOX-HT29 and FOLFOX-HCT116 cell lines. Cells were treated with different concentrations of **7a** and **7b** for 24 h. The whole cell extract was processed for the determination of protein levels by western blot analysis. **Panel A** shows the protein levels of cleaved caspase 3, cleaved PARP 1, BIM, Bax and Bcl2. Normalization of protein loading was assessed by GAPDH. **Panel B** shows the Bax/Bcl2 ration.

Chk1 phosphorylation by **7a** and **7b** is caused only at Ser317 not at Ser345, indicating that ATR may not be a target of **7a** and **7b**. However, this possibility cannot be completely ruled out as the ATR was not included in our kinase profiling assays. It is also possible that Chk1 is indirectly inhibited by proteins, such as Claspin, that serves as a scaffold protein in ATR-mediated Chk1 phosphorylation [72,73]. The down-regulation of Claspin expression have been shown to inhibit Chk1 activation in response to replication stress [74]. Studies are awaited to examine whether **7a-** and **7b**-mediated inhibition of Chk1 phosphorylation is due to down-regulation of Claspin. Furthermore, **7a** and **7b** might down-regulate mammalian TOR complex 1 (mTORC1) activity, that in turn, may down-regulate Chk1 phosphorylation and induce γH2AX phosphorylation [75]. However, we have not yet experimentally verified the role of mTORC1 in **7a**- and **7b**-mediated inhibition of Chk1 phosphorylation.

2.3.9. Treatment of 7a and 7b increases the levels of apoptosis marker proteins in FOLFOX-HT29 and FOLFOX-HCT116 cell lines

In previous studies, increased expression of Bax, an important member of the Bcl2 family, has pro-apoptotic effect [76], and has been implicated in the better survival of colorectal cancer patients [77–79]. On the other hand, increased expression of Bcl2 prevents apoptosis by inhibiting the activity of Bax [80]. Thus, the increased Bax/Bcl2 ratio plays a critical role in determining the susceptibility to apoptosis in cancer cells. We determined the effect of **7a** and **7b** treatments on the expression of apoptotic marker proteins e.g. cleaved caspase 3 and PARAP 1 and then determined their correlation with Bax/Bcl2 ratio in FOLFOX-HT29 and FOLFOX-HCT116 cells. Results showed an increased levels of cleaved caspase 3 and PARP1 in FOLFOX-HT29 and FOLFOX-HCT116 cells after treatment with **7a** and **7b**, suggesting an increased level of apoptosis in these cell lines (Fig. 7A). The apoptotic effect of **7a** and **7b** was further supported by the increased Bax/Bcl2 ratio (Fig. 7A and B).

2.3.10. Drug-like properties of 7a and 7b

With an aim to check to the drug-likeness of our compounds, we explored the Lipinski's parameters [81] for our two potent compounds (**7a** and **7b**) using the "Filter by Lipinski and Veber Rules" embedded in the Discovery Studio (DS) 4.0 client (Accelrys, San Diego, CA, USA), and are summarized in Table 5. According to Lipinski's rule, any compound with the molecular weight (MW) greater than 500 Da, hydrogen bond acceptors (HBAs) more than 10, hydrogen bond donors (HBDs) more than five, and an octanol-water partition coefficient (logP) value more than 5, is likely to have poor absorption or membrane permeation under physiological conditions. Similarly, Veber et al., based on their studies in rats,

Table 5
Predicted Lipinski's and Verber's parameters for **7a** and **7b**.

Compound	logP	MWt	HBA	HBD	TPSA	Rotatable bonds
7a	−0.13	229.7	4	0	10.07	3
7b	1.2	271.3	4	0	10.07	4

Table 4
Effect of **7a** and **7b** on the Chk1 activity in an *in vitro* assay system.

NSC30049 (7a) and ASR352 (7b) Concentration (M)	Percent activity			Saturosporine Concentration (M)
	NSC30049 (7a)	ASR352 (7b)	Staurosporine	
1.00E-04	91.54	90.47	0.31	2.00E-05
3.33E-05	105.37	95.76	−1.28	5.00E-06
1.11E-05	94.37	94.16	1.47	1.25E-06
3.70E-06	106.53	96.66	2.55	3.13E-07
1.23E-06	113.75	95.86	−0.27	7.81E-08
4.12E-07	99.00	105.75	6.54	1.95E-08
1.37E-07	100.06	106.27	9.81	4.88E-09
4.57E-08	92.52	106.18	13.67	1.22E-09
1.52E-08	92.23	90.13	41.24	3.05E-10
5.08E-09	112.15	104.82	55.99	7.63E-11
DMSO	103.06	100.00	96.94	DMSO

Compounds were tested in 10-dose IC_{50} mode with 3-fold serial dilution starting at 100 μM. Control compound, Staurosporine, was tested in 10-dose IC_{50} mode with 4-fold serial dilution starting at 20 μM. Reactions were carried out at 10 μM ATP. Data is presented as % enzyme activity (relative to DMSO controls).

suggested that any compound with rotatable bonds ≤10 would have good oral availability [82]. A closer inspection of Table 5 shows that both **7a** and **7b** showed compliance with the Lipinski's as well as Veber indicators. The topological polar surface area (TPSA), which is an indicator for hydrogen bond forming capability of molecules, was also computationally predicted using the same tool in DS. More than 90% drugs targeting human proteins are reported to have PSA <140 $Å^2$, hence considered to be an important indicator to predict the bioavailability of drug candidates after oral absorption. Both **7a** and **7b** with TPSA around 10 $Å^2$ exhibited compliance with TPSA indicator (Table 5), again suggesting their potential to be developed as drug molecules.

3. Conclusion

In conclusion, SAR based on novel **7a** analogs led to the identification of **7b** which showed comparable potency in inhibiting the growth of CRC bulk, sensitized FOLFOX-resistant, and reduced sphere formation capacity of CRC stem cells. Experiments to evaluate underlying mechanisms of action revealed that **7a** and **7b** abrogated 5-FU-induced S phase, reduced the phosphorylation of Chk1 at S315P, S345P and S296P, increased γH2AX staining, and increased the expression of apoptotic marker proteins. Thus, these compounds have the potential to be developed further as a therapeutic agent that is effective both as a single agent and in combination with 5-FU, with solid mechanistic basis by targeting the Chk1 pathway in 5-FU-resistant CRC heterogeneous bulk and CRC stem cell populations.

4. Experimental

4.1. Chemistry

4.1.1. General

Melting points were recorded on a Fischer-Johns melting point apparatus and are uncorrected. ^{1}H NMR spectra were recorded on a Bruker Advance 500 instrument in $CDCl_3$, operating at 500 MHz. Chemical shifts are reported in δ values (ppm) and *J* values are reported in hertz (Hz). The signals are quoted as s (singlet), d (doublet), t (triplet), m (multiplet), and dd (doublet of doublet). High-resolution MS were recorded on AB Sciex 5600 TripleTOF instrument at Pennsylvania State University, University Park. Experiments were performed under a nitrogen atmosphere in oven-dried glassware. Reagents, starting materials, and anhydrous solvents were purchased from commercial suppliers and were used as received. Reaction courses were monitored by thin-layer chromatography (TLC) on pre-coated silica gel 60 F_{254} aluminum sheets (Merck, Darmstadt, Germany), and the spots were visualized under UV light. The crude reaction products were purified by recrystallization in ethanol-methylene chloride mixture. Tetraazaadamantane (**8a**) triaza-phophaadamanatne (**8b**), various alkyl/alkenyl/aryl halides **9** and phenacyl derivatives **10a-c** were purchased from commercial sources. The purity of the final compounds (≥97%) was quantified by analytical high performance liquid chromatography analysis by comparing the peak areas of the product relative to any impurities. Synthesis of **7a** was accomplished in our laboratory following the procedure of Warmus et al. [83], as described in our recent studies [13].

4.1.2. General procedures for the synthesis of novel azaadamantane NSC30049 analogs (*7a-h*)

A mixture of 1.0 mmol of 1,3,5,7-tetraazaadamantane (**8a**) or 1,3,5-triaza-phosphaadamantane **8b** and alkenyl halides **9a-c** (1.0 mmol) in CH_2Cl_2 (10 ml) was refluxed 6 h (for reaction with **8a**) and 9 h (for reaction with **8b**). After completion of the reaction as indicated by TLC, reaction mass was cooled to room temperature, filtered the residue, and washed with excess methylene dichloride. The crude solid thus obtained was recrystallized in an EtOH/CH_2Cl_2 mixture and was dried under vacuum (1 mm) to afford the corresponding pure analogs **7a-h**.

4.1.3. 1-(4-Chloro-but-2-enyl)-3,5,7-triaza-1-azonia-tricyclo [3.3.1.1^{3,7}]decane; chloride (*7a*)

Yield 92% (0.243 g); white solid; mp 199–201 °C; ^{1}H NMR (500 MHz, D_2O) δ [ppm]: 6.31–6.27 (m, 1H), 5.97–5.93 (m, 1H), 5.08 (s, 6H), 4.71 (s, 3H), 4.54 (d, *J* = 11.0 Hz, 3H), 4.20 (d, *J* = 5.0 Hz, 2H), 3.57 (d, *J* = 6.0 Hz, 2H); ^{13}C NMR (125 MHz, DMSO-d_6) δ [ppm]: 140.6, 117.1, 78.1, 70.13, 57.8, 43.0; HRMS (ESI, M^+) calcd. for $C_{10}H_{18}ClN_4$ 229.1219, found 229.1218.

4.1.4. 1-(3-Phenyl-allyl)-3,5,7-triaza-1-azonia-tricyclo[3.3.1.1^{3,7}] decane; chloride (*7b*)

Yield 90% (0.262 g); white solid; mp 207–209 °C; ^{1}H NMR (600 MHz, DMSO-d_6) δ [ppm]: 7.59 (d, *J* = 7.5 Hz, 2H), 7.41 (t, *J* = 7.5 Hz, 2H), 7.36 (d, *J* = 6.0 Hz, 1H), 6.84 (d, *J* = 16.0 Hz, 1H), 6.47–6.44 (m, 1H), 5.17 (s, 6H), 4.61 (d, *J* = 12.5 Hz, 3H), 4.50 (d, *J* = 12.5 Hz, 3H), 3.67 (d, *J* = 7.5 Hz, 2H); ^{13}C NMR (150 MHz, DMSO-d_6) δ [ppm]: 140.7, 135.8, 129.3, 129.1, 129.1, 127.7, 115.2, 78.1, 71.8, 70.3, 58.0; HRMS (ESI, M^+) calcd. for $C_{15}H_{21}N_4$ 257.1766, found 257.1744.

4.1.5. 1-But-2-enyl-3,5,7-triaza-1-azonia-tricyclo[3.3.1.1^{3,7}]decane; chloride (*7c*)

Yield 82% (0.188 g, as mixture of *E*:*Z* = 7.4:2.6); white solid; mp 227–229 °C; ^{1}H NMR-*E* isomer (600 MHz, DMSO-d_6) δ [ppm]: 6.01–5.96 (m, 1H), 5.63–5.60 (m, 1H), 5.07 (s, 6H), 4.59 (d, *J* = 12.5 Hz, 3H), 4.49–4.45 (m, 3H), 3.45 (d, *J* = 7.5 Hz, 2H), 1.75 (d, *J* = 6.0 Hz, 3H); ^{13}C NMR (150 MHz, DMSO-d_6) δ [ppm]: 139.2, 116.7, 79.6, 70.3, 57.8, 18.4; HRMS (ESI, M^+) calcd. for $C_{10}H_{19}N_4$ 195.1609, found 195.1592.

4.1.6. 7-(4-Chloro-but-2-enyl)-1,3,5-triaza-7-phosphonia-tricyclo [3.3.1.1^{3,7}]decane; chloride (*7d*)

Yield 92% (0.259 g); pale yellow solid; mp 219–221 °C (dec.); ^{1}H NMR (500 MHz, D_2O) δ [ppm]: 6.33–6.28 (m, 1H), 6.02–5.96 (m, 1H), 4.95 (d, *J* = 11.5 Hz, 2H), 4.85 (d, *J* = 12.0 Hz, 2H), 4.61 (d, *J* = 13.5 Hz, 1H), 4.45 (d, *J* = 14.0 Hz, 1H), 4.43–4.21 (m, 4H), 4.00–3.94 (m, 2H), 3.86–3.83 (m, 2H), 3.61 (d, *J* = 7.5 Hz, 2H); ^{13}C NMR (125 MHz, D_2O) δ [ppm]: 80.4, 80.3, 67.91, 67.8, 58.3, 57.8, 51.0, 50.6, 48.6, 24.5.

4.1.7. 7-(3-Phenyl-allyl)-1,3,5-triaza-7-phosphonia-tricyclo [3.3.1.1^{3,7}]decane; chloride (*7e*)

Yield 88% (0.271 g); pale yellow solid; mp 203–205 °C; ^{1}H NMR (500 MHz, DMSO-d_6) δ [ppm]: 7.59 (d, *J* = 6.5 Hz, 2H), 7.59 (t, *J* = 6.0 Hz, 2H), 7.34 (t, *J* = 6.0 Hz, 1H), 6.85 (d, *J* = 13.0 Hz, 1H), 6.47–6.43 (m, 1H), 5.01 (d, *J* = 9.5 Hz, 2H), 4.95 (d, *J* = 9.5 Hz, 2H), 4.52 (d, *J* = 11.0 Hz, 1H), 4.39–4.36 (m, 3H), 3.92–3.90 (m, 2H), 3.86–3.85 (m, 2H), 3.69 (d, *J* = 6.5 Hz, 2H); ^{13}C NMR (125 MHz, DMSO-d_6) δ [ppm]: 141.2, 135.8, 129.3, 129.1, 127.7, 115.3, 78.8, 69.7, 63.8, 52.5, 52.3, 45.9, 45.8; HRMS (ESI, M^+) calcd. for $C_{15}H_{21}N_3P$ 274.1473, found 274.1448.

4.1.8. 7-But-2-enyl-1,3,5-triaza-7-phosphonia-tricyclo[3.3.1.1^{3,7}] decane; chloride (*7f*)

Yield 78% (0.192 g, as mixture of *E*:*Z* = 7.6:2.4); pale yellow solid; mp 249–251 °C; ^{1}H NMR-*E* isomer (500 MHz, DMSO-d_6) δ [ppm]: 6.04–5.99 (m, 1H), 5.66–5.62 (m, 1H), 4.93–4.88 (m, 4H), 4.52 (d, *J* = 15.0 Hz, 1H), 4.39–4.33 (m, 2H), 4.30 (d, *J* = 5.0 Hz, 1H), 3.92 (t, *J* = 14.0 Hz, 2H), 3.84–3.80 (m, 2H), 3.49 (d, *J* = 7.5 Hz, 2H), 1.79 (d,

$J = 6.5$ Hz, 3H); ^{13}C NMR (125 MHz, DMSO-d_6) δ [ppm]: 139.8, 116.8, 78.5, 69.7, 63.6, 52.2, 46.0, 18.6; HRMS (ESI, M^+) calcd. for $C_{10}H_{19}N_3P$ 212.1316, found: 212.1295.

4.1.9. 1-(4-Chloro-butyl)-3,5,7-triaza-1-azonia-tricyclo[3.3.1.1 ^{3,7}] decane; chloride (**7g**)

The mixture of 1,3,5,7-tetraazaadamantane **8a** (1.40 g, 10 mmol) and 1,4-dichlorobutane (1.27 g, 10 mmol) in acetone (10 mL) was refluxed for 24 h. After completion of the reaction as indicated by TLC, reaction mixture was cooled to room temperature, filtered the residue, and washed with excess acetone. The crude solid thus obtained was recrystallized in an EtOH/CH_2Cl_2 mixture and was dried under vacuum (1 mm) to afford the corresponding pure analog **7g**. Yield 87% (0.232 g); white solid; mp 229–231 °C; ^{1}H NMR (500 MHz, D_2O) δ [ppm]: 5.09 (s, 6H), 4.71–4.69 (m, 3H), 4.56–4.53 (m, 3H), 3.63 (t, $J = 6.5$ Hz, 2H), 2.94–2.91 (m, 2H), 1.88–1.77 (m, 4H); ^{13}C NMR (150 MHz, D_2O) δ [ppm]: 81.8, 79.9, 78.4, 78.3, 71.4, 70.1, 69.8, 56.3, 44.2, 43.0, 28.7, 17.0; HRMS (ESI, M^+) calcd. for $C_{10}H_{20}ClN_4$ 231.1376, found: 231.1358.

4.1.10. 1-(3-boronobenzyl)-3,5,7-triaza-1-azonia-tricyclo [3.3.1.13,7]decane; chloride (**7h**)

The mixture of 1,3,5,7-tetraazaadamantane **8a** (0.140 g, 1.0 mmol) and [3-(Chloromethyl)phenyl]boronic acid (0.170 g, 1.0 mmol) in CH_2Cl_2 (10 mL) was refluxed for 24 h. After completion of the reaction as indicated by TLC, reaction mass was cooled to room temperature, filtered the residue, and washed with excess CH_2Cl_2. The crude solid thus obtained was recrystallized in an EtOH/CH_2Cl_2 mixture and was dried under vacuum (1 mm) to afford the corresponding pure analog **7h**.

Yield 75% (0.232 g); white solid; mp 235–237 °C; ^{1}H NMR (600 MHz, DMSO-d_6) δ [ppm]: 8.30–8.20 (brs, 2xOH, 2H), 7.92 (d, $J = 6.0$ Hz, 1H), 7.81 (s, 1H), 7.51–7.46 (m, 2H), 5.05 (s, 6H), 4.58 (d, $J = 10.5$ Hz, 3H), 4.43 (d, $J = 10.0$ Hz, 3H), 4.04 (s, 2H); ^{13}C NMR (150 MHz, DMSO-d_6) δ [ppm]: 138.4, 136.2, 134.4, 128.6, 125.1, 78.1, 73.5, 73.3, 70.3, 70.2, 60.0, 55.4; HRMS (ESI, M^+) calcd. for $C_{13}H_{20}BN_4O_2$ 275.1679, found: 275.1659.

4.1.11. General procedures for the synthesis of novel azaadamantane NSC30049 (**7a**) analogs **11a-c**

A mixture of azaadamantane **8a** (1 mmol) and phenacyl chlorides **10a-c** (1 mmol) in CH_2Cl_2 (10 mL) was refluxed 24 h. After completion of the reaction as indicated by TLC, reaction mass was cooled to 25 °C, the residue was filtered and washed with excess methylene dichloride. The crude solid thus obtained was recrystallized from a mixture of EtOH and CH_2Cl_2 and was further dried under vacuum (1 mm) at 25 °C to afford the corresponding pure **11a-c**.

4.1.12. 1-(2-Oxo-2-phenyl-ethyl)-3,5,7-triaza-1-azonia-tricyclo [3.3.1.1^{3,7}]decane; chloride (**11a**)

Yield 87% (0.255 g); white solid; mp 167–169 °C; ^{1}H NMR (600 MHz, DMSO-d_6) δ [ppm]: 7.99 (d, $J = 6.0$ Hz, 2H), 7.75 (t, $J = 6.0$ Hz, 1H), 7.61 (t, $J = 7.0$ Hz, 2H), 5.42 (s, 6H), 4.95 (s, 2H), 4.67 (d, $J = 10.5$ Hz, 3H), 4.58 (d, $J = 10.5$ Hz, 3H); ^{13}C NMR (150 MHz, DMSO-d_6) δ [ppm]: 191.6, 135.2, 134.9, 129.5, 129.2, 129.2, 128.6, 121.4, 79.5, 72.6, 71.3, 70.7, 59.3, 57.7; HRMS (ESI) calcd. for $C_{14}H_{19}N_4O$ 259.1558, found: 259.1542.

4.1.13. 1-[2-(4-Methoxy-phenyl)-2-oxo-ethyl]-3,5,7-triaza-1-azonia-tricyclo[3.3.1.13,7]decane; chloride (**11b**)

Yield 82% (0.265 g); white solid; mp 182–184 °C; ^{1}H NMR (600 MHz, DMSO-d_6) δ [ppm]: 7.92 (d, $J = 7.0$ Hz, 2H), 7.07 (d, $J = 7.5$ Hz, 2H), 5.43 (s, 6H), 4.80–4.75 (m, 6H), 4.64 (s, 2H), 3.90 (s, 3H); ^{13}C NMR (150 MHz, DMSO-d_6) δ [ppm]: 189.7, 164.8, 131.4, 130.8, 127.0, 114.5, 81.8, 79.4, 71.8, 70.3, 55.8; HRMS (ESI, M^+) calcd. for $C_{15}H_{21}N_4O_2$ 289.1664, found: 289.1640.

4.1.14. 1-(3-Oxo-3-phenyl-propyl)-3,5,7-triaza-1-azonia-tricyclo [3.3.1.13,7]decane; chloride (**11c**)

Yield 77% (0.237 g); white solid; mp 204–206 °C; ^{1}H NMR (600 MHz, DMSO-d_6) δ [ppm]: 8.08 (dd, $J = 7.0$, 1.0 Hz, 2H), 7.71 (t, $J = 6.5$ Hz, 1H), 7.59 (t, $J = 6.5$ Hz, 2H), 5.21 (s, 6H), 4.63 (d, $J = 10.5$ Hz, 3H), 4.52 (d, $J = 10.5$ Hz, 3H), 3.71 (t, $J = 6.5$ Hz, 2H), 3.18 (t, $J = 6.5$ Hz, 2H); ^{13}C NMR (150 MHz, DMSO-d_6) δ [ppm]: 196.9, 136.4, 134.3, 129.2, 128.6, 78.6, 71.5, 70.3, 51.4, 30.0; HRMS (ESI, M^+) calcd. for $C_{15}H_{21}N_4O$ 273.1715, found: 273.1704.

4.2. Biological evaluations

4.2.1. Ethics statement

All procedures performed in this study have been in accordance with the ethical standards of the institutional and/or national research committee and with the 1964 Helsinki declaration and its later amendments or comparable ethical standards.

4.2.2. Cell lines and cell cultures

Human colon cancer cell lines HCT-116 and HT-29 were obtained from the American Type Culture Collection (ATCC, Rockville, MD). Cells were maintained as recommended by ATCC either in McCoy's 5a or Dulbecco's modified Eagle medium (DMEM; 4.5 g/L D-glucose) supplemented with 10% FBS and 1% antibiotic/antimycotic in tissue culture flasks in a humidified incubator at 37 °C in an atmosphere of 95% air and 5% carbon dioxide. The medium was changed two times a week and cells were passaged using 0.05% trypsin/EDTA.

The FOLFOX-resistant HCT-116 and HT29 cell lines were obtained from Dr. Adhip P. Majumdar (John D. Dingell VA Medical Centre, Detroit, MI) [42]. These cells were generated by exposure to clinically relevant doses and schedules. The exposing schedule was for 12 cycles; each cycle lasted for one week. Briefly, the cells were first exposed to FOLFOX (25 μM 5-FU and 0.625 μM oxaliplatin) for 72 h. The surviving cells were then cultured in normal medium without the drugs for 4–5 days. This cycle was repeated 12 times. The surviving cells were then split and exposed to higher doses of FOLFOX (50 μM 5-FU + 1.25 μM oxaliplatin or 100 μM 5-FU + 2.5 μM oxaliplatin) for 2–3 days per week for approximately 4 weeks. Finally, the resistant cells were maintained in normal culture medium containing a low dose of FOLFOX (5 μM 5-FU + 0.125 μM oxaliplatin).

CRC stem cell line, CA2, was obtained from Dr. Emina Huang (Lerner Research Institute, Cleveland, OH), as described in our recent publication [13]. These cells were characterized for the expression of ESA^{high}, ALDH1$^+$, CD44$^+$and CD133$^+$ stem cell markers [43,44]. These cells were maintained in DMEM/F12 (50/50 1X) medium containing, 6 g/ml D-glucose, 1 mg/ml $NaHCO_3$, 4 mg/ml bovine serum albumin, 2 mM glutamate, 25 mg/ml ITS (insulin, transferrin, and selenium), 20 nM progesterone, 9.6 μg/ml putrescine, and 1% antibiotic/antimycotic solution in ultra-low attachment 6-well plates. Cultures were maintained in a humidified incubator at 37 °C in an atmosphere of 95% air and 5% carbon dioxide.

4.2.3. Cell survival assay

The survival of cells was determined by MTT (3-(4,5-Dimethylthiazol-2yl-)-2,5-diphenyltetrazolium bromide) assay (ATCC, Manassas, VA). In principle, the viable cell number is directly proportional to the purple formazan color of the reduced MTT dye, which can be quantitatively measured by spectrophotometry. Briefly, 1500 cells were plated in quadruplets in 96-well flat-bottom

tissue culture plates. After treatment with compounds for certain periods as described in respective figure legends, 10 μl of MTT reagent was added to each well and incubated at 37 °C for 4 h to allow the formation of purple color crystals of formazan. In total, 100 μl of detergent solution was added to each well, and the reaction mixture was incubated in dark for 2–4 h at room temperature. The developed color density was then measured spectrophotometrically at 570 nm using the POLARstar Omega micro-plate reader (BMG Labtech, Inc., Cary, NC).

4.2.4. Spheroid formation assay

Live CA2 cells (100) were seeded in 384-well ultra-low attachment plates. Next, day cells were treated with different concentrations of **7a** and 5-FU either alone or in combination. Cells were incubated for 7 days and the number of spheroids were counted in control and treated groups under an Olympus inverted microscope with a 10 × magnification.

4.2.5. Fluorescence-activated cell sorting (FACS) analysis

For determining the cell cycle profile, cells were plated in 60 mm tissue culture dishes and grown until 60% confluence. Cells were treated with 25 μM 5-FU for 24 h followed by treatment with 20 μM **7a** for an additional 8 h, as described previously [84]. After treatment, cells were harvested at different time intervals, washed with ice-cold PBS and processed for FACS analysis [85,86]. The ranges for G_0/G_1, S, and G_2/M phase arrested and sub-G_1 apoptotic cells were established on the basis of the corresponding DNA content of the histograms. At minimum, 10,000 cells were counted from each sample.

4.2.6. Western blot analysis

The levels of various proteins were determined by Western blot analysis with our previously described procedure [87,88]. The antibodies for phospho-Chk1(Ser317), phospho-Chk1(Ser317), phospho-Chk1(Ser319), phospho-Chk1(Ser345), Chk1, and GAPDH were purchased from Cell Signaling Technology (Danvers, MA).

4.2.7. Kinase activity profiling

To determine whether NSC30049 and ASR352 are Chk1 kinase inhibitors, an *in vitro* Chk1 kinase activity was determined by Eurofins Pharma Discovery Services, Wolverhampton, UK. To further determine whether **7a** and **7b** can inhibit any kinases, a profiling of 366 kinases was tested by Reaction Biology Corp., Malvern, PA.

4.2.8. Statistical analysis

All experiments were repeated at least three times and results were expressed as mean ± SE. One-way analysis of variance (ANOVA) was calculated with Sigma-Plot 9. A one-tailed *t*-test was used to compare any significant differences between control and treated groups. The criterion for statistical significance was $p < 0.05$. For western blotting data, band intensities were measured using ImageJ and normalized with GAPDH.

Acknowledgement

This work was supported partially by the Team Science Project #00110481, University of Florida Shands Cancer Center, Gainesville, FL to SN. AKS thanks the Department of Pharmacology, Penn State College of Medicine, and Penn State Cancer Institute (PSCI) for financial support. The authors thank Dr. Jyh-Ming Lin, Solution Phase NMR Facility at Core Research Facilities of the Penn State College of Medicine for recording NMR spectra, and Organic Synthesis Shared Resource of PSCI. The authors also thank the Centre for High Computing Performance (CHPC) based in Cape Town (South Africa) for access and use of computational resources.

Appendix A. Supplementary data

Supplementary data to this article can be found online at https://doi.org/10.1016/j.ejmech.2018.10.052.

References

[1] C.E. Desch, A.B. Benson 3rd, M.R. Somerfield, P.J. Flynn, C. Krause, C.L. Loprinzi, B.D. Minsky, D.G. Pfister, K.S. Virgo, N.J. Petrelli, O. American Society of Clinical, Colorectal cancer surveillance: 2005 update of an American Society of clinical Oncology practice guideline, J. Clin. Oncol. 23 (2005) 8512–8519.
[2] S. Kosmider, L. Lipton, Adjuvant therapies for colorectal cancer, World J. Gastroenterol. 13 (2007) 3799–3805.
[3] J. Cassidy, J.L. Misset, Oxaliplatin-related side effects: characteristics and management, Semin. Oncol. 29 (2002) 11–20.
[4] H.K. Sanoff, W.R. Carpenter, J. Freburger, L. Li, K. Chen, L.L. Zullig, R.M. Goldberg, M.J. Schymura, D. Schrag, Comparison of adverse events during 5-fluorouracil versus 5-fluorouracil/oxaliplatin adjuvant chemotherapy for stage III colon cancer: a population-based analysis, Cancer 118 (2012) 4309–4320.
[5] W. Zhang, M. Feng, G. Zheng, Y. Chen, X. Wang, B. Pen, J. Yin, Y. Yu, Z. He, Chemoresistance to 5-fluorouracil induces epithelial-mesenchymal transition via up-regulation of Snail in MCF7 human breast cancer cells, Biochem. Biophys. Res. Commun. 417 (2012) 679–685.
[6] M. Izumiya, A. Kabashima, H. Higuchi, T. Igarashi, G. Sakai, H. Iizuka, S. Nakamura, M. Adachi, Y. Hamamoto, S. Funakoshi, H. Takaishi, T. Hibi, Chemoresistance is associated with cancer stem cell-like properties and epithelial-to-mesenchymal transition in pancreatic cancer cells, Anticancer Res. 32 (2012) 3847–3853.
[7] T. Brabletz, A. Jung, S. Spaderna, F. Hlubek, T. Kirchner, Opinion: migrating cancer stem cells - an integrated concept of malignant tumour progression, Nat. Rev. Canc. 5 (2005) 744–749.
[8] S.A. Mani, W. Guo, M.J. Liao, E.N. Eaton, A. Ayyanan, A.Y. Zhou, M. Brooks, F. Reinhard, C.C. Zhang, M. Shipitsin, L.L. Campbell, K. Polyak, C. Brisken, J. Yang, R.A. Weinberg, The epithelial-mesenchymal transition generates cells with properties of stem cells, Cell 133 (2008) 704–715.
[9] X.Y. Han, B. Wei, J.F. Fang, S. Zhang, F.C. Zhang, H.B. Zhang, T.Y. Lan, H.Q. Lu, H.B. Wei, Epithelial-mesenchymal transition associates with maintenance of stemness in spheroid-derived stem-like colon cancer cells, PloS One 8 (2013), e73341.
[10] E. Sanchez-Tillo, O. de Barrios, L. Siles, M. Cuatrecasas, A. Castells, A. Postigo, beta-catenin/TCF4 complex induces the epithelial-to-mesenchymal transition (EMT)-activator ZEB1 to regulate tumor invasiveness, Proc. Natl. Acad. Sci. U.S.A. 108 (2011) 19204–19209.
[11] O. Schmalhofer, S. Brabletz, T. Brabletz, E-cadherin, beta-catenin, and ZEB1 in malignant progression of cancer, Cancer Metastasis. Rev. 28 (2009) 151–166.
[12] T.T. Onder, P.B. Gupta, S.A. Mani, J. Yang, E.S. Lander, R.A. Weinberg, Loss of E-cadherin promotes metastasis via multiple downstream transcriptional pathways, Cancer Res. 68 (2008) 3645–3654.
[13] S. Narayan, A.S. Jaiswal, R. Sharma, A. Nawab, L.V. Duckworth, B.K. Law, M. Zajac-Kaye, T.J. George, J. Sharma, A.K. Sharma, R.A. Hromas, NSC30049 inhibits Chk1 pathway in 5-FU-resistant CRC bulk and stem cell populations, Oncotarget 8 (2017) 57246–57264.
[14] A.I. Kuznetsov, N.S. Zefirov, Azaadamantanes with nitrogen atoms in the bridgehead positions, Russ. Chem. Bull. 58 (1989) 1033–1047.
[15] F. Jimenez-Cruz, H. Rios-Olivares, J.L.G. Gutierrez, Molecular structure of 1-azaadamantanes and 1,3-diazaadamantanes, in: I. Iriepa (Ed.), Structural Analysis of Cyclic Systems, Research Signpost, Trivandrum, 2005, pp. 101–125.
[16] H. Izumi, S. Yamagami, S. Futamura, 1-Azaadamantanes: pharmacological applications and synthetic approaches, Curr. Med. Chem. Cardiovasc. Hematol. Agents 1 (2003) 99–111.
[17] D.P. Becker, D.L. Flynn, R.L. Shone, G. Gullikson, Azaadamantane benzamide 5-HT4 agonists: gastrointestinal prokinetic SC-54750, Bioorg. Med. Chem. Lett 14 (2004) 5509–5512.
[18] L. Shi, M.J.C. Scanio, W.H. Bunnelle, Amimomethyl azaadamantane derivatives and use thereof as selective modulators of the alpha7- neuronal nicotinic acetylcholine receptor (nnrs), PCT Int. Appl. WO 2008118747A1; Chem. Abstr. 149 (2008) 425803.
[19] W.H. Bunnelle, 4-substituted azaadamantane derivatives and methods of use thereof, PCT Int. Appl. WO 2008118745A1; Chem. Abstr. 149 (2008) 425802.
[20] M.R. Schrimpf, D.L. Nersesian, K.B. Sippy, J. Ji, T. Li, L. Shi, Azaadamantane ester and carbamate derivatives and methods of use thereof, PCT Int. Appl. WO 2008118742A1; Chem. Abstr. 149 (2008) 425805.
[21] S.D. Banister, D.T. Yoo, S.W. Chua, J. Cui, R.H. Mach, M. Kassiou, N-Arylalkyl-2-azaadamantanes as cage-expanded polycarbocyclic sigma (sigma) receptor ligands, Bioorg. Med. Chem. Lett 21 (2011) 5289–5292.
[22] A. Demir, R.M. Oguariri, A. Magis, D.A. Ostrov, T. Imamichi, B.M. Dunn, Kinetic characterization of newly discovered inhibitors of various constructs of human T-cell leukemia virus-1 (HTLV-1) protease and their effect on HTLV-1-infected cells, Antivir. Ther. 17 (2012) 883–892.
[23] A.J. Kesel, Synthesis of novel test compounds for antiviral chemotherapy of severe acute respiratory syndrome (SARS), Curr. Med. Chem. 12 (2005)

2095–2162.
[24] J.A. Tanner, B.J. Zheng, J. Zhou, R.M. Watt, J.Q. Jiang, K.L. Wong, Y.P. Lin, L.Y. Lu, M.L. He, H.F. Kung, A.J. Kesel, J.D. Huang, The adamantane-derived bananins are potent inhibitors of the helicase activities and replication of SARS coronavirus, Chem. Biol. 12 (2005) 303–311.
[25] Y. Zhang, Y.T. Di, S.Z. Mu, C.S. Li, Q. Zhang, C.J. Tan, Z. Zhang, X. Fang, X.J. Hao, Dapholdhamines A-D, alkaloids from Daphniphyllum oldhami, J. Nat. Prod. 72 (2009) 1325–1327.
[26] C.R. Zhang, H.B. Liu, T. Feng, J.Y. Zhu, M.Y. Geng, J.M. Yue, Alkaloids from the leaves of Daphniphyllum subverticillatum, J. Nat. Prod. 72 (2009) 1669–1672.
[27] E. Suslov, V.V. Zarubaev, A.V. Slita, K. Ponomarev, D. Korchagina, D.M. Ayine-Tora, J. Reynisson, K. Volcho, N. Salakhutdinov, Anti-influenza activity of diazaadamantanes combined with monoterpene moieties, Bioorg. Med. Chem. Lett 27 (2017) 4531–4535.
[28] T.S. Lo, K.D. Hammer, M. Zegarra, W.C. Cho, Methenamine: a forgotten drug for preventing recurrent urinary tract infection in a multidrug resistance era, Expert Rev. Anti-infe. 12 (2014) 549–554.
[29] X.Q. Li, Q. Xu, J. Luo, L.J. Wang, B. Jiang, R.S. Zhang, D.Y. Shi, Design, synthesis and biological evaluation of uncharged catechol derivatives as selective inhibitors of PTP1B, Eur. J. Med. Chem. 136 (2017) 348–359.
[30] P.Y. Zhang, I.L. Wong, C.S. Yan, X.Y. Zhang, T. Jiang, L.M. Chow, S.B. Wan, Design and syntheses of permethyl ningalin B analogues: potent multidrug resistance (MDR) reversal agents of cancer cells, J. Med. Chem. 53 (2010) 5108–5120.
[31] S. Saha, V. Reddy Ch, S. Xu, S. Sankar, N. Neamati, B. Patro, Synthesis and SAR studies of marine natural products ma'edamines A, B and their analogues, Bioorg. Med. Chem. Lett 23 (2013) 5135–5139.
[32] M.A. Morgan, L.A. Parsels, L. Zhao, J.D. Parsels, M.A. Davis, M.C. Hassan, S. Arumugarajah, L. Hylander-Gans, D. Morosini, D.M. Simeone, C.E. Canman, D.P. Normolle, S.D. Zabludoff, J. Maybaum, T.S. Lawrence, Mechanism of radiosensitization by the Chk1/2 inhibitor AZD7762 involves abrogation of the G2 checkpoint and inhibition of homologous recombinational DNA repair, Cancer Res. 70 (2010) 4972–4981.
[33] A. Gutierrez-Gonzalez, C. Belda-Iniesta, J. Bargiela-Iparraguirre, G. Dominguez, P. Garcia Alfonso, R. Perona, I. Sanchez-Perez, Targeting Chk2 improves gastric cancer chemotherapy by impairing DNA damage repair, Apoptosis Int. J. Program. Cell Death 18 (2013) 347–360.
[34] S.D. Zabludoff, C. Deng, M.R. Grondine, A.M. Sheehy, S. Ashwell, B.L. Caleb, S. Green, H.R. Haye, C.L. Horn, J.W. Janetka, D. Liu, E. Mouchet, S. Ready, J.L. Rosenthal, C. Queva, G.K. Schwartz, K.J. Taylor, A.N. Tse, G.E. Walker, A.M. White, AZD7762, a novel checkpoint kinase inhibitor, drives checkpoint abrogation and potentiates DNA-targeted therapies, Mol. Canc. Therapeut. 7 (2008) 2955–2966.
[35] Z. Xiao, J. Xue, T.J. Sowin, S.H. Rosenberg, H. Zhang, A novel mechanism of checkpoint abrogation conferred by Chk1 downregulation, Oncogene 24 (2005) 1403–1411.
[36] M.A. Morgan, L.A. Parsels, J.D. Parsels, A.K. Mesiwala, J. Maybaum, T.S. Lawrence, Role of checkpoint kinase 1 in preventing premature mitosis in response to gemcitabine, Cancer Res. 65 (2005) 6835–6842.
[37] E. Blackwood, J. Epler, I. Yen, M. Flagella, T. O'Brien, M. Evangelista, S. Schmidt, Y. Xiao, J. Choi, K. Kowanetz, J. Ramiscal, K. Wong, D. Jakubiak, S. Yee, G. Cain, L. Gazzard, K. Williams, J. Halladay, P.K. Jackson, S. Malek, Combination drug scheduling defines a "window of opportunity" for chemopotentiation of gemcitabine by an orally bioavailable, selective ChK1 inhibitor, GNE-900, Mol. Canc. Therapeut. 12 (2013) 1968–1980.
[38] S. Lapenna, A. Giordano, Cell cycle kinases as therapeutic targets for cancer, Nat. Rev. Drug Discov. 8 (2009) 547–566.
[39] L.I. Toledo, M. Murga, R. Zur, R. Soria, A. Rodriguez, S. Martinez, J. Oyarzabal, J. Pastor, J.R. Bischoff, O. Fernandez-Capetillo, A cell-based screen identifies ATR inhibitors with synthetic lethal properties for cancer-associated mutations, Nat. Struct. Mol. Biol. 18 (2011) 721–727.
[40] R.B. Diasio, B.E. Harris, Clinical pharmacology of 5-fluorouracil, Clin. Pharmacokinet. 16 (1989) 215–237.
[41] T. Rajesh, S.A. Azeez, E. Naresh, G. Madhusudhan, K. Mukkanti, Practical one-pot and large-scale synthesis of N-(tert-Butyloxycarbonyl)-3-pyrroline, Org. Process Res. Dev. 13 (2009) 638–640.
[42] Y. Yu, S.S. Kanwar, B.B. Patel, J. Nautiyal, F.H. Sarkar, A.P. Majumdar, Elimination of colon cancer stem-like cells by the combination of curcumin and FOLFOX, Transl. oncol 2 (2009) 321–328.
[43] E.H. Huang, M.J. Hynes, T. Zhang, C. Ginestier, G. Dontu, H. Appelman, J.Z. Fields, M.S. Wicha, B.M. Boman, Aldehyde dehydrogenase 1 is a marker for normal and malignant human colonic stem cells (SC) and tracks SC overpopulation during colon tumorigenesis, Cancer Res. 69 (2009) 3382–3389.
[44] J.E. Carpentino, M.J. Hynes, H.D. Appelman, T. Zheng, D.A. Steindler, E.W. Scott, E.H. Huang, Aldehyde dehydrogenase-expressing colon stem cells contribute to tumorigenesis in the transition from colitis to cancer, Cancer Res. 69 (2009) 8208–8215.
[45] Z. Storchova, D. Pellman, From polyploidy to aneuploidy, genome instability and cancer, Nat. Rev. Mol. Cell Biol. 5 (2004) 45–54.
[46] C.J. Sherr, J. Bartek, Cell cycle-targeted cancer therapies, Annu. Rev. Cell Biol. 1 (2017) 47–57.
[47] C. Holohan, S. Van Schaeybroeck, D.B. Longley, P.G. Johnston, Cancer drug resistance: an evolving paradigm, Nat. Rev. Canc. 13 (2013) 714–726.
[48] D.B. Longley, P.G. Johnston, Molecular mechanisms of drug resistance, J. Pathol. 205 (2005) 275–292.
[49] G. Manic, F. Obrist, A. Sistigu, I. Vitale, Trial Watch, Targeting ATM-CHK2 and ATR-CHK1 pathways for anticancer therapy, Mol. Cell Oncol. 2 (2015) e1012976.
[50] C.J. Sherr, J.M. Roberts, CDK inhibitors: positive and negative regulators of G1-phase progression, Gene Dev. 13 (1999) 1501–1512.
[51] C.C. Mills, E.A. Kolb, V.B. Sampson, Development of chemotherapy with cell-cycle inhibitors for adult and pediatric cancer therapy, Cancer Res. 78 (2018) 320–325.
[52] E. Martino-Echarri, B.R. Henderson, M.G. Brocardo, Targeting the DNA replication checkpoint by pharmacologic inhibition of Chk1 kinase: a strategy to sensitize APC mutant colon cancer cells to 5-fluorouracil chemotherapy, Oncotarget 5 (2014) 9889–9900.
[53] J. Zhang, Q. Dai, D. Park, X. Deng, Targeting DNA replication stress for cancer therapy, Genes 7 (2016) 51.
[54] M. Dobbelstein, C.S. Sorensen, Exploiting replicative stress to treat cancer, Nat. Rev. Drug Discov. 14 (2015) 405–423.
[55] B.B. Zhou, J. Bartek, Targeting the checkpoint kinases: chemosensitization versus chemoprotection, Nat. Rev. Canc. 4 (2004) 216–225.
[56] H. Kitao, M. Iimori, Y. Kataoka, T. Wakasa, E. Tokunaga, H. Saeki, E. Oki, Y. Maehara, DNA replication stress and cancer chemotherapy, Cancer Sci. 109 (2018) 264–271.
[57] M. Berti, A. Vindigni, Replication stress: getting back on track, Nat. Struct. Mol. Biol. 23 (2016) 103–109.
[58] H. Gaillard, T. Garcia-Muse, A. Aguilera, Replication stress and cancer, Nat. Rev. Canc. 15 (2015) 276–289.
[59] M.K. Zeman, K.A. Cimprich, Causes and consequences of replication stress, Nat. Cell Biol. 16 (2014) 2–9.
[60] E. Vesela, K. Chroma, Z. Turi, M. Mistrik, Common chemical inductors of replication stress: focus on cell-based studies, Biomolecules 7 (2017) 19.
[61] S. Skog, B. Tribukait, B. Wallstrom, S. Eriksson, Hydroxyurea-induced cell death as related to cell cycle in mouse and human T-lymphoma cells, Cancer Res. 47 (1987) 6490–6493.
[62] N.C. Walworth, R. Bernards, rad-dependent response of the chk1-encoded protein kinase at the DNA damage checkpoint, Science 271 (1996) 353–356.
[63] S. Rundle, A. Bradbury, Y. Drew, N.J. Curtin, Targeting the ATR-CHK1 Axis in cancer therapy, Cancers 9 (2017) 41.
[64] W.H. Zhang, A. Poh, A.A. Fanous, A. Eastman, DNA damage-induced S phase arrest in human breast cancer depends on Chk1, but G2 arrest can occur independently of Chk1, Chk2 or MAPKAPK2, Cell Cycle 7 (2008) 1668–1677.
[65] A. Blasina, J. Hallin, E. Chen, M.E. Arango, E. Kraynov, J. Register, S. Grant, S. Ninkovic, P. Chen, T. Nichols, P. O'Connor, K. Anderes, Breaching the DNA damage checkpoint via PF-00477736, a novel small-molecule inhibitor of checkpoint kinase 1, Mol. Canc. Therapeut. 7 (2008) 2394–2404.
[66] S. McNeely, C. Conti, T. Sheikh, H. Patel, S. Zabludoff, Y. Pommier, G. Schwartz, A. Tse, Chk1 inhibition after replicative stress activates a double strand break response mediated by ATM and DNA-dependent protein kinase, Cell Cycle 9 (2010) 995–1004.
[67] M. Srivastava, S.C. Raghavan, DNA double-strand break repair inhibitors as cancer therapeutics, Chem. Biol. 22 (2015) 17–29.
[68] I.M. Ward, J. Chen, Histone H2AX is phosphorylated in an ATR-dependent manner in response to replicational stress, J. Biol. Chem. 276 (2001) 47759–47762.
[69] M. Downey, D. Durocher, gammaH2AX as a checkpoint maintenance signal, Cell Cycle 5 (2006) 1376–1381.
[70] K.A. Cimprich, D. Cortez, ATR: an essential regulator of genome integrity, Nat. Rev. Mol. Cell Biol. 9 (2008) 616–627.
[71] E.A. Nam, D. Cortez, ATR signalling: more than meeting at the fork, Biochem. J. 436 (2011) 527–536.
[72] A. Kumagai, W.G. Dunphy, Claspin, a novel protein required for the activation of Chk1 during a DNA replication checkpoint response in Xenopus egg extracts, Mol. Cell. 6 (2000) 839–849.
[73] S.Y. Jeong, A. Kumagai, J. Lee, W.G. Dunphy, Phosphorylated claspin interacts with a phosphate-binding site in the kinase domain of Chk1 during ATR-mediated activation, J. Biol. Chem. 278 (2003) 46782–46788.
[74] C.C. Chini, J. Chen, Human claspin is required for replication checkpoint control, J. Biol. Chem. 278 (2003) 30057–30062.
[75] X. Zhou, W. Liu, X. Hu, A. Dorrance, R. Garzon, P.J. Houghton, C. Shen, Regulation of CHK1 by mTOR contributes to the evasion of DNA damage barrier of cancer cells, Sci. Rep. 7 (2017) 1535.
[76] Z.N. Oltvai, C.L. Milliman, S.J. Korsmeyer, Bcl-2 heterodimerizes in vivo with a conserved homolog, Bax, that accelerates programmed cell death, Cell 74 (1993) 609–619.
[77] L. Zhang, J. Yu, B.H. Park, K.W. Kinzler, B. Vogelstein, Role of BAX in the apoptotic response to anticancer agents, Science 290 (2000) 989–992.
[78] O. Nehls, T. Okech, C.J. Hsieh, T. Enzinger, M. Sarbia, F. Borchard, H.H. Gruenagel, V. Gaco, H.G. Hass, H.T. Arkenau, J.T. Hartmann, R. Porschen, M. Gregor, B. Klump, Studies on p53, BAX and Bcl-2 protein expression and microsatellite instability in stage III (UICC) colon cancer treated by adjuvant chemotherapy: major prognostic impact of proapoptotic BAX, Br. J. Canc. 96 (2007) 1409–1418.
[79] I. Sturm, C.H. Kohne, G. Wolff, H. Petrowsky, T. Hillebrand, S. Hauptmann, M. Lorenz, B. Dorken, P.T. Daniel, Analysis of the p53/BAX pathway in colorectal cancer: low BAX is a negative prognostic factor in patients with resected liver metastases, J. Clin. Oncol. 17 (1999) 1364–1374.
[80] S. Hector, J.H. Prehn, Apoptosis signaling proteins as prognostic biomarkers in

colorectal cancer: a review, Biochim. Biophys. Acta 1795 (2009) 117–129.
[81] C.A. Lipinski, F. Lombardo, B.W. Dominy, P.J. Feeney, Experimental and computational approaches to estimate solubility and permeability in drug discovery and development settings, Adv. Drug Deliv. Rev. 23 (1997) 2–25.
[82] D.F. Veber, S.R. Johnson, H.-Y. Cheng, B.R. Smith, K.W. Ward, K.D. Kopple, Molecular properties that influence the oral bioavailability of drug candidates, J. Med. Chem. 45 (2002) 2615–2623.
[83] J.S. Warmus, G.J. Dilley, A.I. Meyers, A modified procedure for the preparation of 2,5-dihydropyrrole (3-pyrroline), J. Org. Chem. 58 (1993) 270–271.
[84] R. Montano, I. Chung, K.M. Garner, D. Parry, A. Eastman, Preclinical development of the novel Chk1 inhibitor SCH900776 in combination with DNA-damaging agents and antimetabolites, Mol. Canc. Therapeut. 11 (2012) 427–438.
[85] A.S. Jaiswal, B.P. Marlow, N. Gupta, S. Narayan, Beta-catenin-mediated transactivation and cell-cell adhesion pathways are important in curcumin (diferuylmethane)-induced growth arrest and apoptosis in colon cancer cells, Oncogene 21 (2002) 8414–8427.
[86] A.S. Jaiswal, R. Aneja, S.K. Connors, H.C. Joshi, A.S. Multani, S. Pathak, S. Narayan, 9-bromonoscapine-induced mitotic arrest of cigarette smoke condensate-transformed breast epithelial cells, J. Cell. Biochem. 106 (2009) 1146–1156.
[87] S. Narayan, A.S. Jaiswal, Activation of adenomatous polyposis coli (APC) gene expression by the DNA-alkylating agent N-methyl-N'-nitro-N-nitrosoguanidine requires p53, J. Biol. Chem. 272 (1997) 30619–30622.
[88] S. Narayan, A.S. Jaiswal, D. Kang, P. Srivastava, G.M. Das, C.G. Gairola, Cigarette smoke condensate-induced transformation of normal human breast epithelial cells in vitro, Oncogene 23 (2004) 5880–5889.